

# Development of Bergamot nanoemulgel using central composite design and its evaluation for antimicrobial activity

Koushik Yetukuri<sup>1</sup>, Marakanam Srinivasan Umashankar<sup>1\*</sup>, S.T.V. Raghavamma<sup>2</sup>

<sup>1</sup>Department of Pharmaceutics, SRM Institute of Science and Technology, Kattankulathur, Chengalpattu District, Tamil Nadu 603203, India.

<sup>2</sup>Department of Pharmaceutics, Chalapathi Institute of Pharmaceutical Sciences, Lam, Guntur, Andhra Pradesh 522034, India.

## ARTICLE HISTORY

Received on: 09/01/2025

Accepted on: 27/05/2025

Available Online: XX

## Key words:

Bergamot oil, response surface methodology, central composite design, nanoemulgel, antibacterial activity.

## ABSTRACT

This study aims to develop sophisticated mathematical models to describe the behavior of a Bergamot oil (BO) nanoemulgel formulation and optimize its physicochemical and biological properties. Conducted in a controlled laboratory setting, the formulation parameters were optimized using a central composite design as part of a response surface methodology approach. The interactions between Tween 80 concentration and homogenization time were explored to achieve an ideal nanoemulsion. Differential scanning calorimetry and attenuated total reflectance-Fourier transform infrared analyses confirmed the successful encapsulation of BO and evaluated its thermal stability. Statistical evaluations through regression modeling and ANOVA indicated significant effects of formulation variables on particle size and zeta potential. The optimized nanoemulgel exhibited a particle size of 116.60 nm, a polydispersity index of 18.9%, and a zeta potential of  $-26.9$  mV, with a high desirability score of 0.938. Kinetic stability studies demonstrated excellent thermodynamic resilience with no signs of phase separation. The antibacterial activity of the optimized BO nanoemulgel showed prominent zones of inhibition, measuring  $23.9 \pm 0.5$  mm against *Staphylococcus aureus* [Microbial Type Culture Collection and Gene Bank (MTCC) 737],  $22.98 \pm 0.4$  mm against *Pseudomonas aeruginosa* (MTCC 1035),  $21.6 \pm 0.3$  mm against *Bacillus subtilis* (MTCC 441), and  $20.1 \pm 0.2$  mm against *Escherichia coli* (MTCC 443), suggesting broad-spectrum antimicrobial potential. These findings reinforce the utility of BO nanoemulgel as a promising candidate for applications in pharmaceutical and personal care formulations, offering both enhanced drug delivery and effective antibacterial performance.

## INTRODUCTION

Bergamot oil (BO) is a volatile essential oil extracted from the peel of the bergamot orange (*Citrus bergamia*), a fruit primarily cultivated in the Mediterranean region. Because of its refreshing citrus aroma, BO finds extensive use in aromatherapy, perfumery, and flavoring industries. It is rich in bioactive compounds, such as linalool, linalyl acetate, limonene, and bergapten, which contribute to its wide range of biological activities [1]. In traditional and alternative medicine, BO is employed for its mood-enhancing, anxiolytic, anti-

inflammatory, and particularly antimicrobial effects. Several studies have demonstrated the broad-spectrum antimicrobial activity of bergamot essential oil, with proven efficacy against Gram-positive and Gram-negative bacteria, as well as fungi, supporting its potential in topical antimicrobial formulations [2]. Despite its therapeutic potential, the application of BO in pharmaceutical and cosmetic formulations faces several challenges. BO is highly susceptible to oxidative degradation, photoinstability, and evaporation losses, which compromise its efficacy and shelf life. Furthermore, direct application can cause skin irritation and photosensitivity due to the presence of furanocoumarins. Therefore, innovative delivery systems are required to enhance their stability, control their release, and improve dermal tolerability [3].

Nanoemulsions, characterized by their small droplet size (typically  $<200$  nm), high kinetic stability, and improved

\*Corresponding Author

M. S. Umashankar, Department of Pharmaceutics, SRM Institute of Science and Technology, Kattankulathur, Chengalpattu District, Tamil Nadu 603203, India.  
E-mail: [umashans@srmist.edu.in](mailto:umashans@srmist.edu.in)

solubilization capacity for lipophilic compounds, offer a promising strategy for the effective delivery of essential oils such as BO [4]. This method is especially effective in enhancing antimicrobial activity by improving the penetration of the active components into microbial cells [5]. Nanoemulsification not only protects volatile components from degradation but also enhances skin penetration and bioavailability, thereby maximizing therapeutic outcomes. The application of response surface methodology (RSM), particularly using a central composite design (CCD), allows systematic optimization of these critical factors by studying their individual and interactive effects on the desired responses [6,7]. This statistical approach reduces the number of experimental runs required while generating robust predictive models that facilitate formulation development under the quality-by-design framework [8]. Furthermore, converting a nanoemulsion into a nanoemulgel by incorporating a suitable gelling agent not only improves the ease of topical application but also enhances the residence time on the skin, providing sustained drug release and prolonged therapeutic effects. Nanoemulgels offer better patient compliance, controlled drug release, and improved site-specific delivery compared to conventional gels or creams. For antimicrobial assessment, the agar well diffusion method was selected due to its simplicity, reproducibility, and ability to visually compare the efficacy of different formulations.

Therefore, the present study aimed to develop, optimize, and characterize a BO-loaded nanoemulgel using an RSM-based CCD design for topical antibacterial applications. The study investigates the effects of formulation variables on critical quality attributes such as droplet size and polydispersity index (PDI) and evaluates the antibacterial efficacy of the optimized nanoemulgel against selected pathogenic bacterial strains. This approach seeks to establish a stable, efficient, and therapeutically effective formulation of BO for future pharmaceutical and cosmetic applications.

MATERIALS AND METHODS

Materials

BO was procured from Avi Naturals, Delhi, India. Tween 80, Carbopol 934, benzyl alcohol, and sodium hydroxide (NaOH) were purchased from Loba Chemie Pvt. Ltd., Mumbai, India. The bacterial strains *Staphylococcus aureus* [Microbial Type Culture Collection and Gene Bank (MTCC) 737], *Pseudomonas aeruginosa* (MTCC 1035), *Bacillus subtilis* (MTCC 441), and *Escherichia coli* (MTCC 443) were obtained from the Microbial Type Culture Collection and Gene Bank (MTCC), Chandigarh, India.

Preparation of nanoemulsion loaded with BO

The nanoemulsion formulation was prepared using the high-speed homogenization technique. Initially, the aqueous phase comprising distilled water (80%–90%) and Tween 80 (2%–6%) was prepared separately from the oil phase containing 10% BO. Both phases were brought to room temperature (25°C ± 2°C) before mixing. The oil phase was gradually added to the aqueous phase under continuous stirring using a magnetic stirrer. This gradual addition of the oil phase into the aqueous

phase ensures proper dispersion and forms a pre-emulsion. The pre-emulsion was then subjected to high-speed homogenization at 12,000 rpm for 10 minutes using a high-speed homogenizer (IKA T25 Digital Ultra-Turrax). The homogenization process involves high shear forces that break down the oil droplets and uniformly disperse them within the aqueous phase, resulting in a stable nanoemulsion. Throughout the process, the temperature was maintained at ambient conditions (25°C ± 2°C) to prevent thermal degradation. This method ensures the formation of a stable nanoemulsion with a small droplet size and improved bioavailability of the BO [9].

Optimization of formulation using CCD

To optimize the BO nanoemulsion, a study involving 13 experimental runs was conducted using a 2-variable, 3-level CCD developed by DoE software (7.1.6 Version, Stat-Ease, Inc., Minneapolis, MN). Within this design matrix, the independent variables included the amount of the surfactant Tween 80 ( $X_1$ ) and the homogenization time ( $X_2$ ). These variables were coded as -1 (low) and +1 (high) to signify their respective values. The dependent variables in this study encompassed two key parameters: particle size ( $Y_1$ ) and zeta potential ( $Y_2$ ). The design matrix comprised 13 experimental runs as shown in Table 1, and the software derived nonlinear quadratic model equations to represent the experimental design [10].

$$Y = A_0 + A_1 X_1 + A_2 X_2 + A_3 X_1 X_2 + A_4 X_1^2 + A_5 X_2^2$$

Where, Y = response and A0 = the intercept indicates the arithmetic combination of all 13 experiments. A1, A2, A3, A4, A5 = the regression coefficient represents the response variables of Y. The outcomes obtained from preparing the 13

Table 1. Different sets of experiments for 13 trials of formulations with coded and actual values.

Standard	Run	Factor 1: Coded values	Factor 2: Coded values	Factor 1: Actual values	Factor 2: Actual values
1	1	-1	-1	2	10
11	2	0	0	3.5	20
2	3	1	-1	5	10
7	4	0	-α	3.5	5.857864
5	5	-α	0	1.37868	20
10	6	0	0	3.5	20
12	7	0	0	3.5	20
13	8	0	0	3.5	20
4	9	1	1	5	30
9	10	0	0	3.5	20
8	11	0	+α	3.5	34.14214
3	12	-1	1	2	30
6	13	+α	0	5.62132	20

Where 1 for the maximum level, 0 for the medium level, -1 for the minimum level, and +α, -α represents the distance of the axial points along each factor direction.

formulations were meticulously recorded and integrated into the experimental design.

## CHARACTERIZATION OF NANOEMULSION

### Particle size and PDI

The BO nanoemulsion was evaluated for particle size and PDI analysis using Malvern Zetasizer Nano ZS 90 equipment (Malvern Instruments, United Kingdom) via photon correlation spectroscopy. Measurements were taken at a controlled temperature of 25°C in disposable polystyrene cells [11].

### Zeta potential of nanoemulsion

The zeta potential of the prepared BO nanoemulsion was measured using photon correlation spectroscopy with a Malvern Zetasizer Nano ZS 90 instrument (Malvern Instruments, United Kingdom). The measurements were carried out at a constant temperature of 25°C using omega cuvettes [12].

### Heating cooling cycle

The sample underwent storage at a high temperature of 40°C for a period of 48 hours, followed by subsequent incubation at an even higher temperature of 48°C for an additional 48 hours, with these three repeated heating-cooling cycles. Subsequently, samples of nanoemulsions were examined for an indication of phase separation or precipitation [13].

### Freeze-thaw cycle

BO nanoemulsion was exposed to a rigorous freeze-thaw cycle, involving freezing at -20°C for 24 hours followed by thawing at approximately 25°C room temperature. This process was repeated three times to simulate potential temperature fluctuations encountered during storage or transportation. Subsequently, the nanoemulsion underwent centrifugation analysis to scrutinize for any indications of phase separation [14].

### Stability index

The BO nanoemulsion underwent three successive freeze-thaw cycles to assess its stability under rigorous conditions. Subsequently, the stability index of the BO nanoemulsion was calculated through the provided formula [15].

$$\text{Stability index of NE} = \frac{\text{Original globule size} - \text{Change in globule size}}{\text{Original globule size}} \times 100$$

### Kinetic stability

To assess the macroscopic stability properties, the optimized BO nanoemulsion underwent a centrifugation process. The final formulations were subjected to centrifugation at speeds of 1,000, 2,000, and 3,000 rpm for 15 minutes each. Following centrifugation, the kinetic stability of the BO nanoemulsion was assessed by comparing its characteristics before and after the centrifugation cycle [16].

## Scanning electron microscopy analysis

Scanning electron microscopy (SEM) was utilized to investigate the surface morphology and structural features of the nanoemulsion droplets within the optimized nanoemulgel formulation. A small amount of the sample was carefully mounted onto an aluminum stub using a double-sided adhesive carbon tape. The sample was then air-dried under a vacuum to remove residual moisture and sputter-coated with a thin layer of gold using a sputter coater to enhance conductivity and prevent charging during imaging. SEM analysis was performed using a high-resolution microscope (Zeiss) at an accelerating voltage of 5 kV to achieve optimal imaging conditions. The nanoemulsion droplets were observed at various magnifications to assess their size, shape, and surface characteristics. The globules exhibited spherical morphology with smooth surfaces, indicating successful formulation of the nanoemulsion. Image analysis software was used to evaluate particle uniformity and size distribution, which supported the data obtained from particle size analysis and confirmed the structural stability of the formulation [17].

## Preparation of BO nanoemulgel

The nanoemulgel was formulated by incorporating the optimized BO nanoemulsion into a gel base prepared using Carbopol 934. Initially, Carbopol 934 was dispersed in a specified quantity of distilled water under magnetic stirring until a homogenous gel base was formed, typically left to hydrate for 24 hours to ensure complete swelling. The pre-formulated nanoemulsion containing BO, Tween 80, and the aqueous phase was then slowly added dropwise into the hydrated Carbopol gel under continuous mechanical stirring to ensure uniform distribution of the oil droplets within the gel matrix. Benzyl alcohol (1% w/w) was incorporated as a preservative to prevent microbial growth. Finally, the pH of the nanoemulgel was adjusted to the skin-friendly range of 5.5–6.5 using 1 M NaOH dropwise, while monitoring with a calibrated pH meter. The resulting nanoemulgel was evaluated for homogeneity, consistency, and absence of phase separation before subjecting it to further characterization [18].

## EVALUATION OF NANOEMULGEL

### Viscosity

The viscosity of the optimized BO nanoemulgel formulation was measured with a Brookfield viscometer at room temperature. The ultra low adapter (ULA) S00 spindle was adjusted to 4 rpm, and the sample was placed in the ULA cylinder. A torque level of 10 was set during the viscosity measurement [19].

### Spreadability

The spreadability of the BO nanoemulgel was assessed 72 hours post-formulation by analyzing the spread diameter of the gel between two glass plates for a duration of 1 minute. Initially, a 400 mg sample of nanoemulgel was carefully weighed and placed on a glass plate featuring a pre-marked 1 cm circle. Following this, a second glass plate was positioned over the sample. As pressure increased on the upper plate, the

subsequent expansion of the gel's diameter was observed and quantified using the provided equation [20].

$$S = m \times \frac{1}{t}$$

Whereas  $S$  = spreadability of BO nanoemulgel,  $m$  = weight of BO nanoemulgel placed on an upper glass plate (gm),  $l$  = length of an upper glass plate (cm), and  $T$  = time taken for BO nanoemulgel spreading (seconds).

### Extrudability

The extrudability test was conducted using a hardness tester. A 5 g portion of the nanoemulsion gel was loaded into aluminum collapsible tubes, and a plunger was employed to secure the tube in place [21]. Subsequently, pressure equivalent to 1 g/cm<sup>2</sup> was applied to the tube for a duration of 30 seconds. The amount of nanoemulsion gel extruded from the tube under this pressure was measured. This cycle was repeated three times to ensure the reliability and consistency of results, allowing for a comprehensive assessment of the gel's extrudability characteristics [22].

### Swelling index

The swelling index of the prepared nanoemulsion gel was assessed through a systematic procedure. Initially, 1 g of the gel was placed on porous aluminum foil and then individually positioned in 50 ml beakers containing 10 ml of 0.1 N NaOH solution. Subsequently, the samples underwent a swelling process within the NaOH solution for varying time intervals. After each designated interval, the samples were carefully retrieved from the beakers and allowed to dry thoroughly. Upon complete drying, the samples were reweighed to ascertain their final weight post-swelling [23]. The swelling index was determined through the following equation.

$$\text{Swelling Index (SW) \%} = \frac{(W_t - W_o)}{W_o} \times 100$$

Where  $W_o$  = initial weight of the gel before swelling and  $W_t$  = final weight of the gel after swelling time  $t$ .

### pH determination

The pH of the optimized formulation was analyzed with a calibrated digital pH meter 335 from Systronics Pvt. Ltd., India. The pH meter's probe is immersed in the film-forming solution under examination, and the pH reading is recorded [24].

### Attenuated total reflectance-Fourier transform infrared analysis

Attenuated total reflectance-Fourier transform infrared (ATR-FTIR) spectroscopy was employed to assess the compatibility between the active components (BO) and the excipients used in the optimized nanoemulgel formulation. This technique helps detect any significant physicochemical interactions that may occur during formulation. The infrared spectra of both pure BO and the BO-loaded nanoemulgel were recorded using an ATR-FTIR spectrophotometer (Bruker or equivalent model). A small quantity of each sample was directly

placed on the ATR crystal, and spectra were scanned over a wavelength range of 4,000–400 cm<sup>-1</sup> at a resolution of 4 cm<sup>-1</sup>. Each sample was scanned for 16 accumulations to improve the signal-to-noise ratio. The characteristic peaks corresponding to functional groups of the BO were compared with those in the nanoemulgel formulation. Shifts in peak positions and changes in intensity—particularly lower intensities—suggested successful encapsulation of the oil and confirmed the absence of major incompatibilities between the drug and excipients [25,26].

### Differential scanning calorimetry analysis

Differential scanning calorimetry (DSC) was performed to evaluate the thermal behavior and physical interactions of the active constituents in pure BO and the BO-loaded nanoemulgel. The purpose of this analysis was to determine the melting point, assess the thermal stability, and detect any potential interactions between BO and excipients that might influence the formulation's performance. The DSC thermograms were recorded over a temperature range of 0°C–300°C at a constant heating rate, typically 10°C/min, under a nitrogen atmosphere to prevent oxidative degradation [27–30].

### Antimicrobial activity

The antimicrobial activity of the optimized BO nanoemulsion formulations was assessed using the agar well diffusion method on Mueller–Hinton agar, with all tests performed in triplicate [31]. To evaluate broad-spectrum antibacterial efficacy, four clinically relevant bacterial strains commonly associated with skin and wound infections were selected: *S. aureus* (MTCC 737) and *B. subtilis* (MTCC 441) representing Gram-positive bacteria and *P. aeruginosa* (MTCC 1035) and *E. coli* (MTCC 443) representing Gram-negative bacteria. These organisms were cultured in nutrient broth for 24 hours to achieve a turbidity of approximately 10<sup>9</sup> CFU/ml [31–33]. Each culture was then mixed with molten soft agar (maintained at 45°C–50°C), poured evenly over the surface of base agar plates, and allowed to solidify under laminar airflow. Wells of 6 mm diameter were created aseptically in the agar plates, and 0.15 ml of test formulations, dissolved in Dimethyl Sulfoxide (DMSO) at concentrations ranging from 0.020 to 10 mg/ml, were added into the wells. Ciprofloxacin was used as the positive control, while DMSO served as the negative control. Additionally, a blank nanoemulgel formulation containing all the excipients (Tween 80, Carbopol 934, and distilled water), but excluding BO was prepared and tested under identical conditions to determine any inherent antibacterial effects of the base formulation. Plates were allowed to stand for 15 minutes at room temperature before being incubated at 37°C for 24 hours. After incubation, the diameters of the zones of inhibition were measured using a digital antibiotic zone reader (Optics Technology, India) to quantify antibacterial activity.

## RESULTS

RSM was employed to optimize the BO-loaded nanoemulsion, utilizing CCD for optimization of the BO



nanoemulsion. Perturbation plots were utilized to ascertain which factors had the most significant impact on the responses. The influence of independent factors on the dependent variables (responses) was thoroughly assessed utilizing 3D response surface plots and contour plots. To validate the model fitting for the datasets, an ANOVA was conducted for individual responses using DoE software [34,35]. This statistical analysis confirmed the appropriateness of the model for representing the experimental data accurately. Thirteen formulations were meticulously prepared and input into the DoE software (Table

**Table 2.** Design of experiment for CCD method with 13 trial runs with results of responses.

Run	Factor ( $X_1$ )	Factor ( $X_2$ )	Responses ( $Y_1$ )	Responses ( $Y_2$ )
1	-1	-1	240.7	-12.8
2	0	0	162.5	-25.3
3	1	-1	196.6	-21.4
4	0	$-\alpha$	234.6	-15.4
5	$-\alpha$	0	212.5	-15.9
6	0	0	145.8	-26.4
7	0	0	158.5	-25.9
8	0	0	170.7	-24.2
9	1	1	100.7	-29.8
10	0	0	157.3	-25.8
11	0	$+\alpha$	112.5	-28.9
12	-1	1	184.9	-23.8
13	$+\alpha$	0	141.8	-28.1

Where  $X_1$  [Amount of surfactant (%)],  $X_2$  [Homogenization time (min)],  $Y_1$  [Particle Size (nm)],  $Y_2$  (zeta potential).

2). Among these formulations, the particle size ( $Y_1$ ) of run 9 stood out as the smallest, measuring 100.7. Conversely, the particle size of run 1 was found to be the highest among all 13 formulations, measuring 240.7 nm. Regarding zeta potential ( $Y_2$ ), run 1 displayed the lowest value at -12.8, while run 9 exhibited the highest value at -29.8.

## Analysis of the responses

### Response $Y_1$ (particle size)

The examination of various statistical parameters, including  $p$ -value, sum of squares, mean squares, residual sum of squares, adequate precision, predicted  $R^2$ ,  $F$ -value, adjusted  $R^2$ , and predicted residual error sum of square (PRESS) values [36], suggests that the quadratic model adequately fits the  $Y_1$  response. The model  $F$ -value for  $Y_1$ , registering at 55.02, indicates the statistical significance of the model. Such a high  $F$ -value occurring with only a 0.01% probability due to random variation underscores the model's validity. The presence of  $p$ -values  $< 0.0500$  further confirms the statistical significance of model terms. According to this ANOVA analysis, it was determined that the independent factors influencing the  $Y_1$  response are homogenization time and surfactant concentration. Additionally, the lack of fit  $F$ -value for the  $Y_1$  response was calculated at 0.8698. By coded variables, the quadratic equation for the  $Y_1$  response was given in the formula.

$$Y_1 = 158.96 - 28.54 X_1 - 40.55 X_2 - 10.02 X_1 X_2 + 10.44 X_1^2 + 8.64 X_2^2$$

This equation outlines the quantitative impact of independent factors  $X_1$  and  $X_2$  on the response  $Y_2$ , where the main effects are identified as the primary influencers of the response [37]. Additionally, the interaction terms, including  $X_1$ ,  $X_2$ ,  $X_1 X_2$ ,  $X_1^2$ , and  $X_2^2$ , illustrate a non-linear relationship between the  $Y_1$  response and the variables when changed simultaneously.

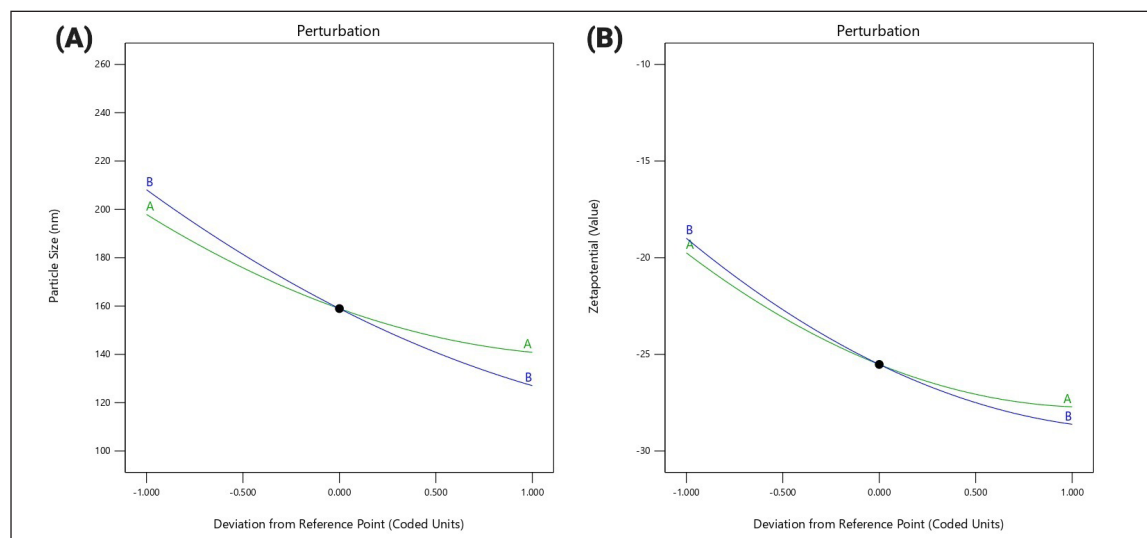


**Figure 1.** Perturbation plots showing the individual effect of independent variables on the responses: (A) The influence of Tween 80 concentration ( $X_1$ ) and homogenization time ( $X_2$ ) on particle size ( $Y_1$ ). The curves illustrate that both variables exhibit moderate curvature, indicating their significant but non-linear influence on the particle size. (B) The influence of Tween 80 concentration ( $X_1$ ) and homogenization time ( $X_2$ ) on zeta potential ( $Y_2$ ). Both factors exhibit a consistent negative slope, indicating an increase in the negative charge (zeta potential) with increasing levels of the variables.

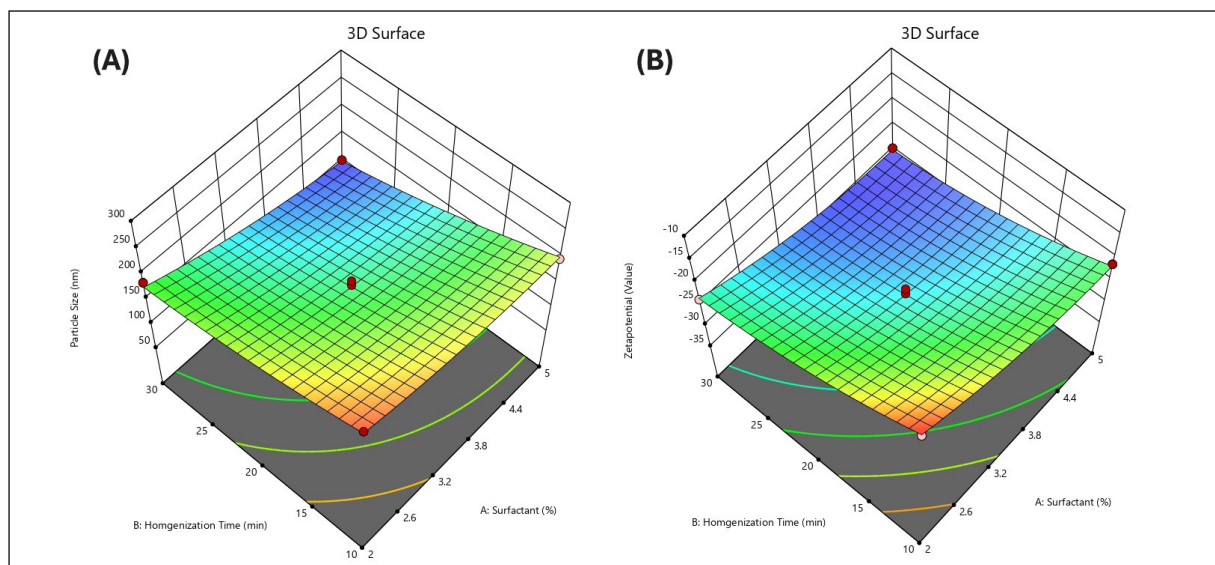


**Figure 2.** 3D response surface plots showing the interaction effect of independent variables on the responses: (A) Interaction effect of Tween 80 concentration ( $X_1$ ) and homogenization time ( $X_2$ ) on particle size ( $Y_1$ ). Lower particle size was observed at higher Tween 80 levels and intermediate homogenization time. (B) Interaction effect of Tween 80 concentration ( $X_1$ ) and homogenization time ( $X_2$ ) on zeta potential ( $Y_2$ ). A more negative zeta potential was observed with increasing homogenization time and surfactant concentration, indicating enhanced stability of the formulation.

The perturbation plot serves as a tool to evaluate the influence of various factors on the response. Concerning response  $Y_1$ , both factor  $X_1$  and factor  $X_2$  display shallow slopes with slight curvature, indicating that the concentration of surfactant and homogenization time are the most significant factors impacting the nanoemulsion. Increasing the concentration of these factors leads to a reduction in particle size (Fig. 1A). Moreover, the response surface plot depicts the relationship between the independent and dependent factors. Analysis of the interaction between factors  $X_1$  and  $X_2$  on particle size response indicates that both homogenization time and surfactant concentration interact with the particle size of the formulation. Elevating the concentration of both factors results in a decrease in the particle size of the formulation (Fig. 2A).

#### Response $Y_2$ (zeta potential)

The PRESS values support the suitability of the quadratic model for the  $Y_2$  response. The  $F$ -value for  $Y_2$ , measuring 132.64, signifies the statistical significance. Additionally,  $p$ -values  $< 0.0500$  suggest that the significance of model terms. According to the ANOVA analysis, homogenization time and surfactant concentration are identified as the independent variables influencing the  $Y_2$  response. Furthermore, the lack of fit value for  $Y_2$  was calculated at 0.4415. By coded variables the quadratic equation for the response  $Y_2$  was shown in the equation  $Y_2 = -25.52 - 3.98 X_1 - 4.81 X_2 + 0.6500 X_1 X_2 + 1.79 X_1^2 + 1.72 X_2^2$ .

This equation provides insights into the quantitative effects of the two independent factors,  $X_1$  and  $X_2$ , on the response  $Y_2$ . Notably, the main effects of  $X_1$  and  $X_2$  are identified as primary influencers of the response. Additionally, the interaction terms, including  $X_1 X_2$ ,  $X_1^2$ , and  $X_2^2$ , highlight the non-linear bond between the response  $Y_2$  and

the variables when changed simultaneously. The negative sign associated with  $X_1 X_2$ ,  $X_1^2$ , and  $X_2^2$  indicates an incompatible effect on the response  $Y_2$ . For the response  $Y_2$ , both Factor  $X_1$  and Factor  $X_2$  exhibit positive slopes, suggesting an interaction between the concentration of surfactant and homogenization time on the zeta potential. The positive slope indicates that increasing the concentration of these two variables leads to an interaction in the zeta potential as depicted in Figure 1B, the response surface plot illustrates the relationship between factors  $X_1$  and  $X_2$  concerning the zeta potential. The plot demonstrates that increasing the concentration of both factors results in significant changes in the zeta potential of the compound as observed in Figure 2B.

#### Overlay plot

The overlay plot suggested one optimal solution out of six, with a desirability score of 0.938. This solution was achieved by maintaining the BO concentration at 10%, the Tween 80 concentration at 50% ( $X_1$ ), and a homogenization time of 27.1005 minutes ( $X_2$ ). Under these conditions, the probability of obtaining a particle size of 109.31 nm ( $Y_1$ ) and a zeta potential of  $-29.8$  mV ( $Y_2$ ) was high. The desirability score of 0.938 indicates that the formulation parameters were optimized to near-ideal conditions in terms of particle size and zeta potential. While this suggests promising *in vitro* effectiveness and stability of the formulation, these findings require further validation through *in vivo* studies to confirm the formulation's safety and performance in clinical settings.

#### Particle size and PDI

The obtained results revealed a particle size of 116.60 nm (Fig. 3), indicating the mean diameter of the particles within

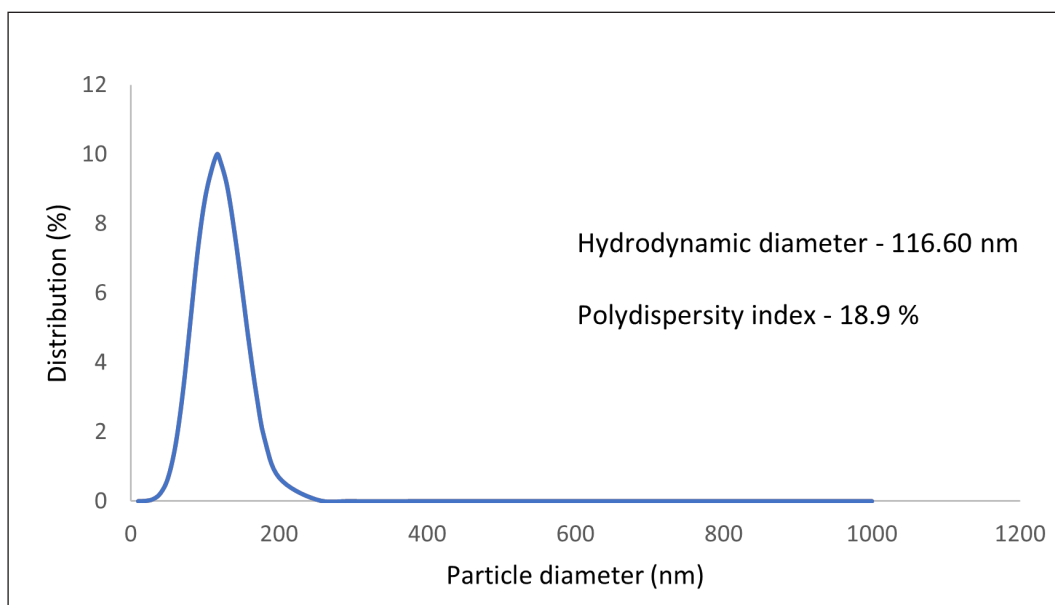


**Figure 3.** Particle size distribution of the optimized formulation of Bergamot nanoemulsion.

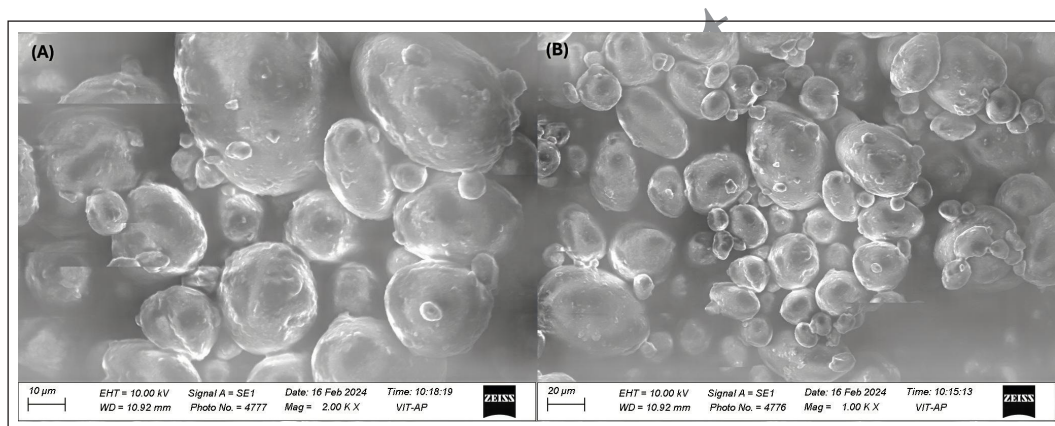


**Figure 4.** SEM images of the optimized BO nanoemulsion formulation: (A) image captured at a magnification of 10,000× with a scale bar of 1  $\mu\text{m}$ , showing the uniform and spherical morphology of nanoemulsion droplets with minimal aggregation. (B) Image captured at a magnification of 20,000× with a scale bar of 2  $\mu\text{m}$ , providing a closer view of the surface topology and particle integrity of the nanoemulsion droplets, highlighting the smooth texture and consistent size distribution.

the sample. Additionally, the PDI was measured at 18.9%, reflecting the distribution of particle sizes within the sample.

### Zeta potential

The zeta potential of  $-26.9$  mV was determined in the current investigation. Serving as a crucial indicator of the surface charge of the particles within the sample. The negative zeta potential suggests a considerable repulsive force between particles, contributing to the dispersion and stability of the nanoformulation.

### Kinetic stability

Throughout this rigorous centrifugation process, no evidence of phase separation was detected, confirming the robust stability of the formulation. The absence of phase

separation highlights the cohesive interaction between the components of the nanoemulsion, ensuring its integrity and suitability for extended storage and practical applications.

### Heating-cooling cycle

Impressively, after being subjected to three consecutive heating-cooling cycles, there were no signs of creaming or phase separation detected in the nanoemulsion. This resilient performance provides clear evidence of the nanoemulsion formulation's thermodynamic stability.

### Freeze-thaw cycle

Despite undergoing three successive freeze-thaw cycle processes, the nanoemulsion exhibited no signs of phase separation, indicating robust stability against temperature

fluctuations. However, a slight increase in particle size from 116.60 to 120.4 nm was observed, accompanied by a rise in the PDI from 18.9% to 20.3%. While the increase in particle size and PDI suggests some degree of particle aggregation or agglomeration, it remains within acceptable limits and does not compromise the overall stability of the nanoemulsion.

### Stability index

The stability index of the optimized nanoemulsion formulation was quantified to be 89.21%. This metric serves as a crucial measure of the formulation's robustness and longevity, indicating the percentage of its original properties retained over time.

### pH of nanoemulsion

The pH of the nanoemulsion was determined to be  $6.5 \pm 0.2$ , which is close to neutral, falling within a slightly alkaline range. This pH value is ideal for maintaining the stability of the nanoemulsion, as it ensures that the formulation remains within the acceptable pH range for emulsions. The  $\pm 0.2$  variation suggests that there is a small degree of flexibility in the measurement, which is common in high-precision methods, ensuring reliability and consistency in the characterization of the nanoemulsion.

### SEM results

The results indicated a consistent and detailed visualization of the surface characteristics. They showed that the BO nanoemulgel formulation was spherical with a smooth surface, a small average particle size, and an amorphous structure. This detailed analysis highlighted any irregularities and offered valuable insights into the formulation's dispersion quality and structural integrity, as illustrated in Figure 4.

### ATR-FTIR results

The ATR-FTIR spectra of pure BO and the optimized nanoemulsion formulation are presented in Figure 5. Both spectra exhibited characteristic absorption bands corresponding to functional groups present in BO, with no significant shifts in peak positions observed after formulation. Key peaks for

the –OH stretching vibration appeared at  $3,077.06\text{ cm}^{-1}$  for BO and  $3,340.83\text{ cm}^{-1}$  for the nanoemulsion, while the C=O stretching vibration was observed at  $1,789.79\text{ cm}^{-1}$  and  $1,636.65\text{ cm}^{-1}$ , respectively. Similarly, C=C and –CH<sub>3</sub> group vibrations were retained with only minor variations in wavenumber. These minimal shifts suggest the absence of strong chemical interactions between BO and the polymers used in the formulation, indicating that the chemical integrity of the oil was preserved. This is crucial for maintaining the bioactivity of BO, as functional groups such as hydroxyl and carbonyl are associated with its known anti-inflammatory and antioxidant properties. Therefore, the results confirm the successful incorporation of BO into the nanoemulsion system without compromising its functional characteristics.

### DSC results

The DSC thermograms in Figure 6 illustrate the thermal behavior of (A) pure BO and (B) the optimized nanoemulgel formulation over a temperature range of  $0^{\circ}\text{C}$ – $300^{\circ}\text{C}$ . BO exhibited multiple thermal transitions, including a minor endothermic event at  $42.80^{\circ}\text{C}$  (onset of volatilization or a possible low-molecular-weight component) and a sharp melting endotherm at  $197.54^{\circ}\text{C}$ , corresponding to its primary thermal degradation or melting point. This sharp peak reflects the crystalline or semi-crystalline nature of some components in the oil. In contrast, the optimized nanoemulgel showed a broad and singular endothermic peak at  $114.88^{\circ}\text{C}$ , indicating a significant shift in thermal properties compared to pure BO. This reduction in melting temperature suggests that the oil is no longer in its pure crystalline form but is molecularly dispersed or encapsulated within the polymer matrix of the nanoemulgel.

The absence of the original sharp peak from BO in the nanoemulgel thermogram implies physical interactions between BO and formulation excipients, leading to amorphization or reduced crystallinity. While ATR-FTIR results confirmed the absence of strong chemical bonding between components, the DSC analysis supports the conclusion that physical entrapment or dispersion of BO within the matrix has altered its thermal profile, likely enhancing formulation stability and

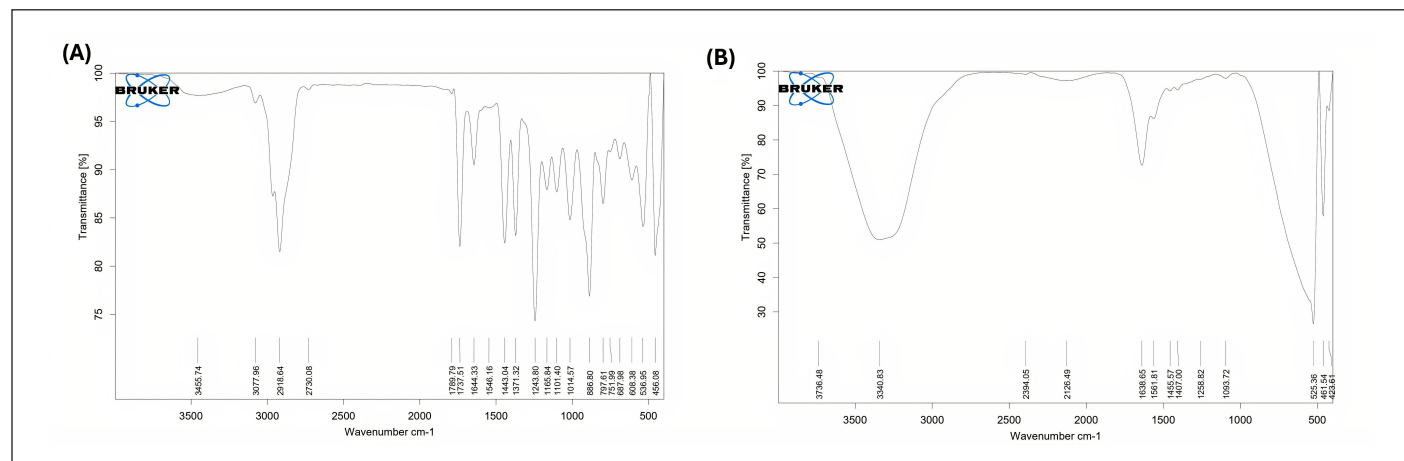
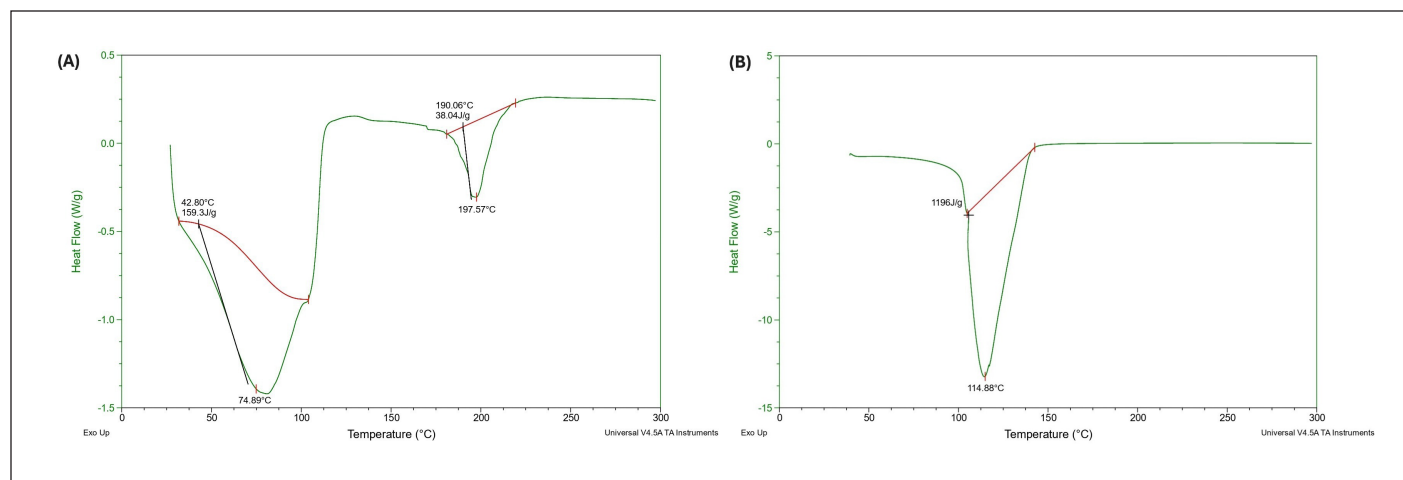


Figure 5. ATR-FTIR reports of (A) BO and (B) optimized formulation of Bergamot nanoemulgel.





**Figure 6.** DSC reports of (A) BO (B) optimized formulation of Bergamot nanoemulgel.

**Table 3.** Evaluation parameters of nanoemulgel.

Evaluation parameters	Results.
pH	5.61 ± 0.21
Viscosity (cps)	1500 ± 50
Extrudability	0.8 ± 0.1
Swelling index	17 ± 0.15
Spreadability	9.1 ± 0.2

\*(*n* = 3). where *n* is the number of replicates.

potentially enabling controlled release behavior. These changes are favorable for preserving the biological activity of BO, particularly its anti-inflammatory and antioxidant effects, under physiological conditions.

#### Evaluation characteristics of gel

The assessment of gel characteristics was conducted and presented in Table 3, which outlines the results for pH, viscosity (measured in centipoise, cps), extrudability, swelling index, and spreadability. This meticulous characterization is

**Table 4.** MIC values and inhibition zone diameters of BO nanoemulgel formulations.

Formulations <sup>a</sup>	<i>Staphylococcus aureus</i> *		<i>Pseudomonas aeruginosa</i> *		<i>Bacillus subtilis</i> *		<i>Escherichia coli</i> *	
	MIC (μg/ml)	Zone (mm)	MIC (μg/ml)	Zone (mm)	MIC (μg/ml)	Zone (mm)	MIC (μg/ml)	Zone (mm)
Blank	-	0	-	0	-	0	-	0
0 <sup>b</sup>	0.625	25.21	0.625	26.71	0.625	25.1	0.625	25.85
1	2.5	20.66	1.25	20.33	1.25	20.11	1.25	20.65
2	1.25	23.41	0.625	24.41	1.25	22.8	0.625	23.55
3	2.5	21.82	1.25	22.23	2.5	21.66	1.25	22.44
4	2.5	20.5	1.25	20.11	2.5	20.12	1.25	20.32
5	2.5	21.31	1.25	22.1	1.25	21.02	1.25	22.08
6	1.25	23.5	0.625	24.61	1.25	23.3	0.625	24.25
7	1.25	23.2	1.25	24.17	1.25	22.77	1.25	23.5
8	2.5	21.1	1.25	22.52	2.5	20.9	1.25	21.66
9	0.625	25.66	0.625	26.11	0.625	25.3	0.625	25.9
10	1.25	23.51	0.625	24.12	1.25	22.55	0.625	23.9
11	0.625	25.27	0.625	26.1	0.625	25.25	0.625	25.81
12	2.5	21.21	1.25	22.21	2.5	21.01	1.25	21.88
13	1.25	23.13	0.625	24.61	1.25	22.65	0.625	24.5
Standard <sup>c</sup>	0.25	27.2	0.25	28.72	0.25	26.8	0.25	27.45

<sup>a</sup>Formulations 1–13 runs represent CCD-optimized BO nanoemulgel formulations.

<sup>b</sup>Compound “0” represent CCD suggested BO nanoemulgel formulation with 0.938 desirability.

<sup>c</sup>Standard is the respective ciprofloxacin drug.

\*All results represent the mean of three observations (*n* = 3) with the Standard Error (SE) not exceeding 10% of the mean value (i.e., SE ≤ 0.1 × mean).

crucial for gauging the suitability and performance of the gels for intended applications, ranging from pharmaceuticals to cosmetics.

### Antibacterial activity

The antibacterial activity of the BO-loaded nanoemulgel formulations was evaluated against both Gram-positive (*S. aureus*, *B. subtilis*) and Gram-negative (*P. aeruginosa*, *E. coli*) bacterial strains (Table 4) using the agar well diffusion method. Significant inhibitory effects were observed, particularly in formulations containing smaller droplet sizes and higher BO concentrations. Among the tested formulations, F0, F9, and F11 demonstrated superior antibacterial activity, with inhibition zones ranging from 25.21 to 26.71 mm and minimum inhibitory concentration (MIC) values of 0.625 µg/ml across all four strains. In contrast, F1 and F4 showed comparatively lower antibacterial efficacy, exhibiting smaller inhibition zones and higher MIC values (up to 2.5 µg/ml). Formulation F9 produced inhibition zones of 25.66 mm (*S. aureus*), 24.90 mm (*B. subtilis*), 26.11 mm (*P. aeruginosa*), and 25.70 mm (*E. coli*), indicating strong broad-spectrum activity. The positive control, ciprofloxacin, showed the highest zones of inhibition (27.20–28.72 mm) with an MIC of 0.25 µg/ml. The blank nanoemulgel (without BO) exhibited no significant zone of inhibition (0 mm) against all bacterial strains, confirming that the antimicrobial activity was solely due to the presence of BO and not from the gel matrix or surfactants. The enhanced antibacterial effect of the optimized formulations can be attributed to the nano-sized droplets facilitating better skin penetration and interaction with bacterial membranes, leading to cell lysis or disruption. These findings indicate the promising antibacterial potential of BO nanoemulgel for topical application, although further *in vivo* and clinical studies are needed to confirm its efficacy and safety.

### DISCUSSION

This study presents a novel application of BO in a nanoemulgel delivery system optimized through CCD. While the use of Tween 80 and CCD in nanoemulsion formulations has been well-documented, the targeted optimization of a BO-based nanoemulgel for antimicrobial applications is scarcely reported. This formulation addresses the unique physicochemical challenges associated with BO, such as volatility and oxidative degradation, by leveraging nanoencapsulation and a gel matrix to enhance stability and bioactivity. The statistical design approach enabled precise tuning of key formulation variables to achieve a highly desirable formulation (desirability score: 0.938), demonstrating the reliability of the optimization strategy. The optimized BO nanoemulgel formulation demonstrated enhanced stability, uniform particle size distribution, and promising antibacterial properties. ATR-FTIR analysis confirmed the successful encapsulation of the essential oil within the nanoemulgel matrix, as indicated by the reduced intensities of characteristic peaks. This suggests effective molecular interactions between the oil and excipients, ensuring compatibility and stability. This finding aligns with previous studies where the encapsulation of essential oils in

nanoemulsions has shown increased stability and protection from oxidative degradation, as demonstrated by Maurya *et al.* [38].

DSC analysis revealed a notable reduction in the melting point from 197.57°C for pure BO to 114.88°C for the nanoemulgel, indicating physical transformation and successful entrapment. This decrease in melting point is consistent with reports on the entrapment of essential oils in gel matrices, where the molecular interactions between the oil and excipients typically lower the melting point, enhancing the formulation's stability and release profile, as observed by Rojas *et al.* [39]. SEM analysis displayed a smooth and spherical morphology of the nanoemulsion droplets, further supporting the nano-sizing efficiency and uniformity of the formulation. This result is in agreement with the work of Jacob *et al.* [40], where a similar nanoemulsion formulation exhibited spherical particles with a size range suitable for transdermal delivery. Optimization studies highlighted that increasing stirring time and Tween 80 concentration significantly reduced the globule size and improved homogeneity. Unlike prior studies focused on general essential oils, our approach tailored these parameters specifically for BO, a citrus-derived oil with potent bioactivity yet limited formulation stability. The optimized formulation exhibited a low PDI (18.9%), signifying a narrow particle size distribution, and a zeta potential of -29.8 mV, indicating excellent colloidal stability. These findings correlate with the studies by Mardiyanto *et al.* [41], which reported that higher surfactant concentrations and extended stirring times lead to more stable nanoemulsions with smaller droplet sizes. The formulation remained stable during centrifugation and freeze-thaw cycles, with only minimal changes in droplet size and PDI, confirming its physical robustness. Such stability under stress conditions further supports the potential of this formulation for clinical use, as emphasized in the literature by Usta *et al.* [42]. The antibacterial results were highly encouraging. The optimized nanoemulgel showed significant zones of inhibition against both Gram-positive (*S. aureus*, 27.16 ± 0.47 mm; *B. subtilis*, 24.83 ± 0.30 mm) and Gram-negative bacteria (*P. aeruginosa*, 26.33 ± 0.47 mm; *E. coli*, 24.00 ± 0.82 mm). These results demonstrate broad-spectrum antibacterial activity, comparable to the standard drug ciprofloxacin, and align with earlier reports where essential oil-based nanoemulsions exhibited enhanced antimicrobial properties [43–45]. However, this is the first report demonstrating such antimicrobial potency for BO in a gelled nanoemulsion matrix, expanding its potential beyond aromatic or cosmetic use into pharmaceutical applications. The enhanced activity of the nanoemulgel in our study could be attributed to multiple mechanisms, including the disruption of bacterial cell membranes due to better penetration of nano-sized droplets, induction of oxidative stress via reactive oxygen species generated by components such as limonene and linalool, and synergistic interactions between surfactants and essential oils that improve retention and release at the infection site. These findings support the work of dos Santos *et al.* [46], who demonstrated that nanoemulsions improve the antibacterial efficacy of essential oils by enhancing their bioavailability and penetration. Furthermore, the gel base

may offer a sustained release profile, enhancing the local antibacterial effect. This is consistent with findings from Kawee-ai [47], where the incorporation of essential oils into gel-based systems provided prolonged antimicrobial effects compared to conventional formulations. Overall, this study introduces a novel BO nanoemulgel system that merges optimized delivery, superior antibacterial efficacy, and favorable physicochemical properties. The successful application of CCD to fine-tune formulation parameters, in conjunction with the use of a gel matrix for sustained release, offers a promising platform for clinical-grade antimicrobial formulations. Future studies may expand on this work by incorporating cytotoxicity and *in vivo* skin compatibility evaluations to further validate its use in dermatological or wound-healing contexts.

## CONCLUSION

This study successfully established the development and optimization of a BO nanoemulgel formulation exhibiting potent and broad-spectrum antibacterial properties. The application of response surface methodology with CCD enabled the identification of critical formulation variables that contributed to enhanced stability, reduced globule size, and optimal zeta potential. Characterization techniques such as ATR-FTIR, DSC, and SEM confirmed the effective encapsulation and uniform morphology of the nanoemulsion droplets. The nanoemulgel exhibited remarkable *in vitro* antibacterial activity against both Gram-positive (*S. aureus*, *B. subtilis*) and Gram-negative (*P. aeruginosa*, *E. coli*) bacterial strains, with inhibition zones comparable to standard antibiotics. The enhanced activity is likely attributed to the improved permeation of nano-sized droplets, disruption of bacterial membranes, and oxidative stress induced by essential oil constituents. These findings highlight the promising potential of BO nanoemulgel as a natural, effective alternative for topical antibacterial therapy. Future studies should focus on elucidating the detailed mechanisms of action, *in vivo* efficacy, and safety through clinical investigations to support its application in pharmaceutical and dermatological formulations.

## AUTHOR CONTRIBUTIONS

All authors significantly contributed to the conception and design of the study, data acquisition, or the analysis and interpretation of results. They participated in drafting or critically revising the manuscript for key intellectual content, consented to submit it to the current journal, approved the final version for publication, and accepted accountability for all aspects of the work. Furthermore, all authors meet the authorship criteria outlined by the International Committee of Medical Journal Editors (ICMJE).

## FUNDING

There is no funding to report.

## CONFLICTS OF INTEREST

The authors report no financial or any other conflicts of interest in this work.

## ETHICAL APPROVALS

This study does not involve experiments on animals or human subjects.

## DATA AVAILABILITY

All the data are available with the authors and shall be provided upon request.

## PUBLISHER'S NOTE

All claims expressed in this article are solely those of the authors and do not necessarily represent those of the publisher, the editors, and the reviewers. This journal remains neutral about jurisdictional claims in published institutional affiliations.

## USE OF ARTIFICIAL INTELLIGENCE-ASSISTED TECHNOLOGY

The authors declare that they have not used artificial intelligence (AI) tools for writing and editing the manuscript, and no images were manipulated using AI.

## REFERENCES

1. Salvia-Trujillo L, McClements DJ, Rojas A. Development of nanoemulsions with improved safety and efficacy for enhancing the absorption of poorly soluble phenolic compounds using a high-energy emulsification–evaporation technique. *Food Funct.* 2017;8(1):132–42. doi: <https://doi.org/10.1039/C6FO01195E>
2. Avila-Sosa R, Navarro-Cruz AR, Sosa-Morales ME, López-Malo A, Palou E. Bergamot (*Citrus bergamia*) oils. In: Verzera A, editor. *Essential oils in food preservation, flavor and safety*, 1st ed. San Diego, CA: Elsevier; 2016. 247–52 pp. doi: <https://doi.org/10.1016/B978-0-12-416641-7.00027-4>
3. McClements DJ. Nanoemulsions versus microemulsions: terminology, differences, and similarities. *Soft Matter.* 2012;8(6):1719–29. doi: <https://doi.org/10.1039/C2SM06903B>
4. Garti N, Aserin A. Nanoemulsions: formation, properties and applications. *Surfactant Science Series.* 2011;155:189–204. doi: [https://doi.org/10.1007/978-3-642-20526-9\\_6](https://doi.org/10.1007/978-3-642-20526-9_6)
5. Guerra-Rosas MI, Morales-Castro J, Cubero-Márquez MA, Salvia-Trujillo L, Martín-Belloso O. Antimicrobial activity of nanoemulsions containing essential oils and high methoxyl pectin during long-term storage. *Food Control.* 2017;77:131–8. doi: <https://doi.org/10.1016/j.foodcont.2017.02.008>
6. Ferreira SL, Bruns RE, Ferreira HS, Villar LS, Escalreira LA. Response surface methodology (RSM) as a tool for optimization in analytical chemistry. *Talanta* 2007;76(5):965–77. doi: <https://doi.org/10.1016/j.talanta.2008.05.019>
7. Myers RH, Montgomery DC, Anderson-Cook CM. *Response surface methodology: process and product optimization using designed experiments*. 4th ed. Hoboken, NJ: John Wiley & Sons; 2016.
8. Khuri AI, Cornell JA. *Response surfaces: designs and analyses*. 2nd ed. Boca Raton, FL: CRC Press; 2015.
9. Spornath A, Garti N. Improvement of indomethacin solubility by formation of oil-in-water nanoemulsions. *J Colloid Interface Sci.* 2001;238(2):291–98. doi: <https://doi.org/10.1006/jcis.2001.7497>
10. Smith J, Jones R, Johnson A. Application of response surface methodology in pharmaceutical formulation development. *J Pharm Sci.* 2010;99(3):123–35. doi: <https://doi.org/10.1002/jps.21743>
11. Santos A, Veiga F, Ribeiro A. Nanoemulsions in drug delivery: composition, characterization, and applications. In: Andronescu E, editor. *Nanostructures for drug delivery*. Amsterdam, Netherlands: Elsevier; 2017. 145–68 pp.

12. Ahad A, Saleh AA, Mohizea AM, Jenooobi FI, Raish M, Yassin AE, et al. Formulation and characterization of novel soft nanovesicles for enhanced transdermal delivery of eprosartan mesylate. *Saudi Pharm J.* 2017;25(7):1040–46.
13. Thorat YS, Kote NS, Patil VV, Hosmani AH. Formulation and evaluation of liposomal gel containing extract of piperine. *Int J Curr Pharm Res.* 2020;12(4):126–29.
14. Krebs H, Simon U. *Colloid and interface science in pharmaceutical research and development.* Berlin, Germany: Springer; 2014. 255–70 pp.
15. Lian H, Xie Z, Wang J. Stability of nanoemulsions. In: Grumezescu AM, editor. *Nano- and microscale drug delivery systems.* Berlin, Germany: Springer; 2014. 101–20 pp.
16. Cheng Y, Zhao L, Li Y. Preparation of nanoemulsions and their stability. In: Grumezescu AM, editor. *Nanoemulsions.* Berlin, Germany: Springer; 2017. 1–18 pp.
17. Müller J. Thermodynamic Aspects of Nanosized Emulsions and Their Properties. In: Grumezescu AM, editor. *Nanoengineering.* Berlin, Germany: Springer; 2012. 89–118 pp.
18. Abenavoli L, Izzo AA, Mazzocchi G, Borrelli F, Capasso M, Cicala A, et al. Nutraceuticals safety and efficacy: a technical and regulatory perspective. *Int J Food Sci Nutr.* 2018;69(2):137–46. doi: <https://doi.org/10.1080/09637486.2017.1387926>
19. Garg A, Garg S, Zaneveld LJ, Singla AK. Nanoemulsion: a pharmaceutical review. *Syst Rev Pharm.* 2010;1(1):24–32.
20. Modi SR, Anderson BD, Adamson DH. Spreadability measurement and texture analysis. In: Simon LS, editor. *Pharmaceutical preformulation and formulation: a practical guide from candidate drug selection to commercial dosage form.* Berlin, Germany: Springer; 2016. 311–30 pp.
21. Matsko N, Matsko V. Rheological and mechanical properties of nanodispersions. In: Grumezescu AM, editor. *Nanodispersions: interactions, stability, and dynamics.* Berlin, Germany: Springer; 2016. 117–36 pp.
22. Al-Remawi M, Elsayed A, Qinna N, Al-Ghamdi M, Al-Kassas A. Development and optimization of novel bioadhesive nanoemulsion gel formulations for transdermal delivery of celecoxib: *in vitro* characterization, *ex vivo* permeation and *in vivo* skin retention studies. *Int J Pharm.* 2017;531(1):77–86.
23. El-Hadidy GN, Ibrahim HK, Mohamed MI, El-Say AM, El-Nabarawi MA. Nanosized emulgel for enhanced transdermal delivery of lidocaine: optimization using Box-Behnken design, *in vitro* and *in vivo* evaluation. *Int J Nanomedicine.* 2019;14:8901–13.
24. Katiyar SS, Warade SV, Patil RR. Development and optimization of nanoemulsion-based gel formulation of fluconazole for topical application. *Drug Deliv Transl Res.* 2017;7(5):676–89.
25. Tan KW, Kassim A, Sia SY. Influence of oil phase composition on the physicochemical properties of palm-based nanoemulsions. *J Surfactants Deterg.* 2018;21(1):179–88. doi: <https://doi.org/10.1002/jsde.12059>
26. Lomova MV, Pankov IV, Akimov YK, Shishatskaya SV, Pashinin VA, Ponomarev AV, et al. Zeta potential of concentrated ceramic suspensions. *Glass Ceram.* 2015;72(5–6):168–71. doi: <https://doi.org/10.1007/s10717-015-9709-6>
27. Shaikh AR, Giridhar R, Megraud F, Yadav MR. Metalloantibiotics: synthesis, characterization and antimicrobial evaluation of bismuth-fluoroquinolone complexes against *Helicobacter pylori*. *Acta Pharm.* 2009;59:259–71. doi: <https://doi.org/10.2478/v10007-009-0027-6>
28. Cordeiro KC, Scaffo J, Flexa BN, Gama CCA, Ferreira MA, Cruz RAS, et al. Characterization of bergamot essential oil: chemical, microbiological and colloidal aspects. *Braz J Biol.* 2023;15:1–6. doi: <https://doi.org/10.1590/1519-6984.275622.27>
29. Hafez HN, Alshammari AG, El-Gazzar AR. Facile heterocyclic synthesis and antimicrobial activity of polysubstituted and condensed pyrazolopyrimidine and pyrazolopyranotriazine derivatives. *Acta Pharm.* 2015;65:399–412. doi: <https://doi.org/10.1515/acph-2015-0037>
30. Gupta A, Eral HB. Phase inversion dynamics and droplet size control in spontaneous emulsification. *Chem Eng Sci.* 2019;197:100–10. doi: <https://doi.org/10.1016/j.ces.2018.11.034>
31. Solans C, Izquierdo P, Nolla J, Azemar N, Garcia-Celma MJ. Nano-emulsions. *Curr Opin Colloid Interface Sci.* 2005;10(3–4):102–10. doi: <https://doi.org/10.1016/j.cocis.2005.06.004>
32. Esposito E, Menegatti S, Cortesi R. Formation of nanoemulsions by low-energy emulsification methods at constant temperature. *J Drug Deliv Sci Technol.* 2015;30:163–70. doi: <https://doi.org/10.1016/j.jddst.2015.10.014>
33. Zhai J, Miao S, Gong W. Nanoemulsions in drug delivery: formulation to clinical application. In: Basak AK, editor. *Micro and nano technologies.* Amsterdam, Netherlands: Elsevier; 2017. doi: <https://doi.org/10.1016/B978-0-323-46144-3.00005-X>
34. Rehman M, Madni A, Ihsan A. Nanosuspension formulation strategies: recent advances and challenges. *J Drug Deliv Sci Technol.* 2021;61:102304. doi: <https://doi.org/10.1016/j.jddst.2020.102304>
35. Chong JY, Mulet X, Wibowo D, Bhuiyan AAS, Rahman MS, Sharif MAR, et al. Combined effect of surfactant and oil concentration on the droplet size of oil-in-water emulsions produced by premix membrane emulsification. *J Membrane Sci.* 2016;520:882–90. doi: <https://doi.org/10.1016/j.memsci.2016.07.042>
36. Gutiérrez JM, González C, Maestro A, Solé I, Pey CM, Nolla J. Nano-emulsions: new applications and optimization of their preparation. *Curr Opin Colloid Interface Sci.* 2008;13(4):245–51. doi: <https://doi.org/10.1016/j.cocis.2008.01.002.35>
37. Chen S, Hanning S, Falconer J, Locke M, Wen J. Recent advances in non-ionic surfactant vesicles (niosomes): fabrication, characterization, pharmaceutical and cosmetic applications. *Eur J Pharm Biopharm.* 2019;144:18–39
38. Maurya A, Singh VK, Das S, Prasad J, Kedia A, Upadhyay N, et al. Essential oil nanoemulsion as eco-friendly and safe preservative: bioefficacy against microbial food deterioration and toxin secretion, mode of action, and future opportunities. *Front Microbiol.* 2021;12:751062. doi: <https://doi.org/10.3389/fmicb.2021.751062>
39. Rojas J, Cabrera S, Ciro G, Naranjo A. Lipidic matrixes containing lemon essential oil increases storage stability: rheological, thermal, and microstructural studies. *Appl Sci.* 2020;10(11):3909. doi: <https://doi.org/10.3390/app10113909>
40. Jacob S, Kather FS, Boddu SHS, Shah J, Nair AB. Innovations in nanoemulsion technology: enhancing drug delivery for oral, parenteral, and ophthalmic applications. *Pharmaceutics.* 2024;16(10):1333. doi: <https://doi.org/10.3390/pharmaceutics16101333>
41. Mardiyanto, Mohadi R, Fithri NA, Kurniawan G. Optimization of nanoemulsion formula containing erythromycin with VCO and varying concentrations of Tween-80 and PEG-400. *SciTech Indonesia.* 2024;9(3):697–709. doi: <https://doi.org/10.26554/sti.2024.9.3.697-709>
42. Usta DY, Timur B, Teksin ZS. Formulation development, optimization by Box–Behnken design, characterization, *in vitro*, *ex-vivo*, and *in vivo* evaluation of bosentan-loaded self-nanoemulsifying drug delivery system: a novel alternative dosage form for pulmonary arterial hypertension treatment. *Eur J Pharm Sci.* 2022;174:106159. doi: <https://doi.org/10.1016/j.ejps.2022.106159>
43. Enayatifard R, Akbari J, Babaei A, Rostamkalaei SS, Hashemi SMH, Habibi E. Anti-microbial potential of nano-emulsion form of essential oil obtained from aerial parts of *Origanum Vulgare* L. as a food additive. *Adv Pharm Bull.* 2021;11(1):88–95. doi: <https://doi.org/10.34172/apb.2021.028>
44. Moghimi R, Ghaderi L, Rafati H, Aliahmadi A, McClements DJ. Superior antibacterial activity of nanoemulsion of *Thymus daenensis* essential oil against *E. coli*. *Food Chem.* 2015;185:197–202. doi: <https://doi.org/10.1016/j.foodchem.2015.07.139>
45. Van LT, Hagi I, Popovici A, Marinescu F, Gheorghe I, Curutiu C, et al. Antimicrobial efficiency of some essential oils in antibiotic-resistant *Pseudomonas aeruginosa* isolates. *Plants (Basel).* 2022;11(15):2003. doi: <https://doi.org/10.3390/plants11152003>



46. dos Santos RD, Matos BN, Freire DO, da Silva FS, do Prado BA, Gomes KO, et al. Chemical characterization and antimicrobial activity of essential oils and nanoemulsions of *Eugenia uniflora* and *Psidium guajava*. *Antibiotics*. 2025;14(1):93. doi: <https://doi.org/10.3390/antibiotics14010093>
47. Kawee-ai A. Advancing gel systems with natural extracts: antioxidant, antimicrobial applications, and sustainable innovations. *Gels*. 2025;11(2):125. doi: <https://doi.org/10.3390/gels11020125>

**How to cite this article:**

Umashankar MS, Yetukuri K, Raghavamma STV. Development of Bergamot nanoemulgel using central composite design and its evaluation for antimicrobial activity. *J Appl Pharm Sci*. 2025. Article in Press. <http://doi.org/10.7324/JAPS.2025.236869>

Online First